water

MDPI

Article

Responses of Soil and Ammonia Nitrogen Loss Rates to Hydraulic Parameters under Different Slope Gradients and Rainfall Intensities

Hao Yang [1], Chenchen Wei [2], Guanghui Sun [1], Xueqing Tao [1], Yitong Wang [1] and Weimin Xing [1,*]

[1] College of Hydraulic Science and Engineering, Yangzhou University, Yangzhou 225009, China; mz120231162@stu.yzu.edu.cn (H.Y.); 15037634186@163.com (G.S.); 15252575515@163.com (X.T.); wangyitong@yzu.edu.cn (Y.W.)
[2] Agricultural Water Conservancy Department, Changjiang River Scientific Research Institute, Wuhan 430010, China; weichenchen@cau.edu.cn
* Correspondence: xingweimin@yzu.edu.cn

Abstract: Soil erosion and the consequent loss of nutrients have consistently been significant factors contributing to land degradation and nonpoint source pollution. While runoff serves as the primary carrier for nutrient loss, the hydraulic processes governing the mechanisms of nutrient loss remain not entirely clear. This paper aims to investigate the impacts of rainfall intensity and the slope gradient on hydraulic parameters, soil loss rates, and ammonia nitrogen loss rates, with the objective of determining the optimal hydraulic parameters for more accurate predictions of soil erosion and nutrient loss rates. A series of simulated rainfall experiments with three rainfall intensities (25, 50, and 75 mm min^{-1}) and four slope gradients (8.7%, 17.6%, 26.8%, and 36.4%) were conducted on a 5 m × 10 m slope. The results indicated that the flow velocity, shear stress, stream power, unit stream power, and unit energy all increased with the increase in slope gradient or rainfall intensity. The water depth decreased with an increase in the slope gradient but increased with an increase in the rainfall intensity. Laminar flow occurred in all experiments (Reynolds number < 500). Only the overland flow under a 25 mm h^{-1} rainfall intensity and 8.7% slope gradient was subcritical flow (Froude number < 1). Hydraulic parameters, the soil loss rate, and ammonia nitrogen loss rate could be all expressed as the product of rainfall intensity and slope power function, with R^2 ranging from 0.949 to 0.997. The average soil loss rate and process soil erosion rate could both be fitted using the power function of hydraulic parameters, with the optimal fitting parameter being stream power (R^2 = 0.980 and 0.909). The average ammonia nitrogen loss rate exhibited a linear relationship with the hydraulic parameters, and the optimal fitting parameter was also stream power (R^2 = 0.933). However, there were relatively low correlations between hydrodynamic parameters and the ammonia nitrogen loss rate (R^2 = 0.450–0587). Our results contribute to a deeper understanding of the hydraulic processes involved in nutrient loss.

Keywords: rainfall simulation; stream power; sandy soil; soil loss; ammonia nitrogen loss

check for updates

Citation: Yang, H.; Wei, C.; Sun, G.; Tao, X.; Wang, Y.; Xing, W. Responses of Soil and Ammonia Nitrogen Loss Rates to Hydraulic Parameters under Different Slope Gradients and Rainfall Intensities. *Water* **2024**, *16*, 230. https://doi.org/10.3390/w16020230

Academic Editor: Maria Mimikou

Received: 4 December 2023
Revised: 3 January 2024
Accepted: 6 January 2024
Published: 9 January 2024

1. Introduction

Land resources are one of the fundamental resources for human survival and development [1]. However, during the course of human development and the exploitation of land resources, there is an acceleration in soil erosion, presenting significant challenges for the sustainable development of agricultural production and ecological environment construction. Notably, the highest rates of soil erosion are commonly observed on sloping agricultural lands [2]. Soil erosion on these agricultural slopes not only results in the depletion of the surface soil layer but also transports nutrients from the soil into rivers and lakes through runoff, causing agricultural nonpoint source pollution, restricting soil utilization, and impeding agricultural development.

The exploration of the hydraulic characteristics of rainfall-induced runoff erosion on slopes and its impacts on sediment transport patterns has long been a foundational element in erosion mechanics. After the formation of runoff, the movement of soil particles on slopes is predominantly influenced by the dynamics of overland flow. Runoff-induced erosion can be conceptualized as an energy-consuming process under the motion of overland flow [3,4]. Soil erosion happens when the erosive force of slope runoff surpasses the critical shear stress dispersion effect of soil particles, and sediment content in the runoff falls below its sediment-carrying capacity [5,6]. As the sediment content in the runoff progressively increases, the flow velocity decreases, and the energy of overland flow is harnessed for transporting newly generated sediment. Once the sediment content exceeds the energy of the flow, sediment deposition occurs, leading to a decrease in the flow velocity and establishment of a dynamic equilibrium. Slope runoff also triggers the migration of soil nutrients to the surface soil layer by dissolution, convection, and convection–diffusion effects, which may be highly related with the hydraulic parameters such as flow velocity and flow regime. Consequently, understanding the responses of hydrodynamic processes to the nutrient loss process is crucial for implementing rational control measures for soil and nutrient loss [7].

Commonly employed characteristic parameters in the dynamic process of slope overland flow erosion encompass the flow velocity, water depth, Froude number, Reynolds number, shear stress, stream power, and so on [8–10]. The flow velocity of runoff significantly affects the size of the runoff erosion and sediment-carrying capacity [11]. The Reynolds number is a dimensionless criterion characterizing the viscous effects, while the Froude number represents the ratio between inertial forces and gravity [12]. Shear stress and stream power are commonly used to assess soil erosion rates and characterize the critical dynamic conditions under which soil erosion occurs. Mahmoodabadi et al. [13] observed a linear relationship between soil detachment capacity and runoff stream power. Wu et al. [14] proposed that a linear function could best predict the relationship between soil erosion rates and shear stress and stream power. Wang et al. [15] found that hillside erosion could be adequately modeled using either the power function of shear stress or the linear function of stream power by considering variables such as rainfall intensity, slope, and vegetation cover. Wang et al. [16] noted that the erosion rate could be effectively described using a power function of flow velocity through indoor simulated rainfall experiments. In summary, hydraulic parameters can be effectively characterized using either the linear or power function to describe soil erosion processes [17–19]. However, there is limited research on the impact of hydraulic parameters on nutrient loss. Guo et al. [20] found that the ratio of Manning's roughness coefficient to the average flow depth is a reliable predictor of rill erosion and unit solute transport rate in both flume and field experiments. This suggests a substantial connection between hydraulic parameters and soil detachment, as well as nutrient transport. However, all these studies have drawn conclusions about the hydraulic characteristics based on the average state of the entire slope for the entire rainfall event. Slope overland flow, as a three-dimensional, nonconstant, and nonuniform variable flow, exhibits highly complex flow patterns. There is limited research on how hydraulic parameters influence the soil erosion process during rainfall events.

Slope and rainfall intensity are the two most crucial parameters influencing hydraulic parameters of overland flow [14,19,21,22]. Shen et al. [23] demonstrated that the slope flow velocity and Reynolds number exhibit upward trends with an increasing rainfall intensity and slope gradient. Guo et al. [20] observed a consistent rise in the flow velocity, runoff depth, and Reynolds number as rainfall intensity increased with inflow, coupled with simulated rainfall. Therefore, the purpose of this paper is threefold: 1. Investigate the impact of different slope gradients and rainfall intensities on hydraulic parameters, soil erosion rates, and ammonia nitrogen loss; 2. Develop predictive equations for hydraulic parameters, soil erosion rates, and ammonia nitrogen loss based on the slope and rainfall intensity; 3. Establish predictive equations for soil erosion rates and ammonia nitrogen loss based on hydraulic parameters, and compare the differences in predictive equations using average values and process values. This paper will help determine the optimal hydraulic parameters for more accurate predictions of soil erosion and nutrient loss rates.

2. Materials and Methods

2.1. Soil and Slope Preparation

This field experiment took place at HeLinGe'Er, Hohhot, Inner Mongolia, China (40°12′ N, 111°41′ E). The climate in this region is characterized as a temperate, semi-arid, continental monsoon climate, with an annual average temperature of 6.2 °C. The average annual rainfall is 392.8 mm, and the maximum daily rainfall is 99.1 mm. The runoff plots are 5 m wide and 10 m long, with slopes of 8.7%, 17.6%, 26.8%, and 36.4%, respectively. There is no vegetation growth on the slope, and no soil conservation measures have been implemented. Soil samples were collected at five locations on each runoff plot with an "S" shape, and measurements were taken for soil particle size, soil water content, bulk density, pH, organic matter, and total nitrogen content. Particle size analysis was conducted using a Malvern laser particle size analyzer. The results show that the soil contains 89.6% sand (>0.020 mm), 5.4% silt (0.02–0.002 mm), and 5.0% clay (<0.002 mm). According to the international soil texture classification standard, the soil in the study area is classified as sandy soil. Soil bulk density was measured using the cutting ring method. The soil pH value is determined by using a pH electrode to measure the suspension with a soil-to-water ratio of 1:2.5. The total nitrogen content and organic matter in the soil is measured using the semimicro Kjeldahl method and $K_2Cr_2O_7$ oxidation at 180 °C, respectively. The basic physical and chemical properties of the soil samples are given in Table 1.

Table 1. Basic physical and chemical properties of the test soil samples.

Soil Type	Soil Texture (%)			Soil Bulk Density (g cm^{-3})	pH	Organic Matter (g kg^{-1})	Total Nitrogen (g kg^{-1})
	Sand/% (2.0–0.02 mm)	Silt/% (0.02–0.002 mm)	Clay/% (<0.002 mm)				
Sandy	89.6 ± 0.4	5.4 ± 0.4	5.0 ± 0.3	1.45 ± 0.09	8.40 ± 0.16	2.81 ± 0.07	0.166 ± 0.02

2.2. Rainfall Simulation

Rainfall simulation devices consist of a reservoir, pump, PVC pipes, nozzles, and runoff tank (Figure 1). Three-sided sprinkler nozzles are arranged every 5 m in each side. The opening angle of each nozzle ranges from 0 to 360°. The corner nozzles have a set angle of 90°, while the middle nozzles have a set angle of 180°. Each nozzle can be independently controlled for opening and closing, allowing for the adjustment of rainfall intensity by changing the number of nozzle switches and flow rates. Before each rainfall simulation, rainfall intensity is calibrated using 20 cm diameter runoff buckets. Forty runoff buckets are placed on the slope for each calibration, subject to a 15 min rainfall period for the calculation of both rainfall intensity and uniformity. The calibration will be stopped only when the difference between the actual and set rainfall intensities is within 5%, and the measured rainfall uniformity exceeds 85%, thereby satisfying the requirements of simulated rainfall. The median raindrop diameter is determined using the speckle method and is found to be 1.4 mm. The rainfall height is set at 3.2 m. According to the modified Newton formula, raindrops could reach their terminal velocities before hitting the ground. The calculated rainfall kinetic energy is 13.52 J m^{-2}. The rainfall intensities are 25, 50, and 75 mm h^{-1}, with a rainfall duration of 50 min. Based on long-term rainfall data, the return periods are 0.16, 1, and 3.57 years, respectively, reflecting different rain intensities (moderate, heavy, and storm) in this region.

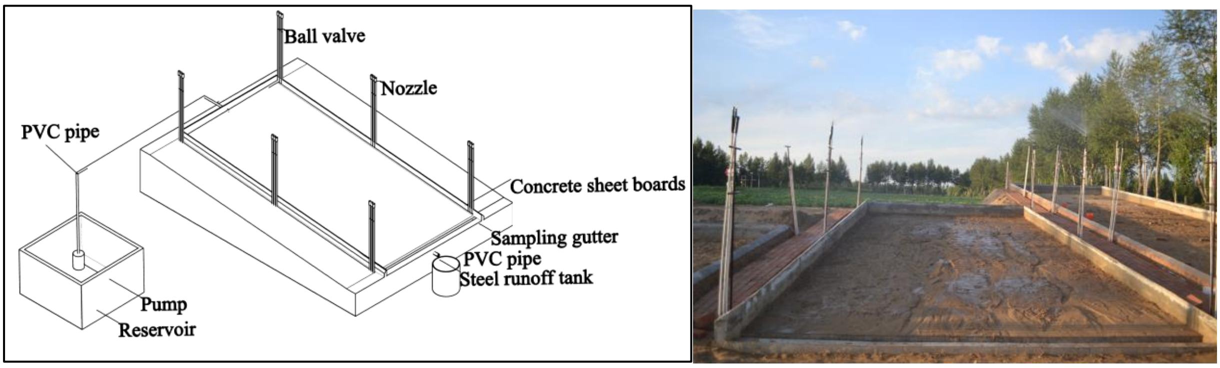

Figure 1. Sketch of the slope and simulated rainfall system.

2.3. Experimental Procedure

The simulated rainfall experiment involved three rainfall intensities (75, 50, and 25 mm h^{-1}) and four slope gradients (8.7%, 17.6%, 26.8%, and 36.4%). A rake was used to level and roughen the slope surface. To ensure consistent initial moisture content on the slope, rainfall at an intensity of 20 mm h^{-1} was applied until the initial generation of runoff 12 h before the actual rainfall. One hour before the start of rainfall, dissolved urea was evenly sprayed on the slope. The amount of urea applied followed local corn planting standards, amounting to 0.03 kg m^{-2}. The simulated rainfall was conducted at 6 a.m. to eliminate the influence of wind.

During simulated rainfall, the times of initial runoff were recorded, and runoff samples were collected in small buckets for one minute. Subsequently, runoff samples were collected every 5 min, with a sampling duration of one minute each time. After the formation of a continuous and stable flow, $KMnO_4$ was used as a tracer to measure the average flow velocity at 4–6 m on the slope. To minimize the impact of the tracer on the ammonia nitrogen concentration, flow velocity measurements were generally conducted after the collection of runoff samples. After rainfall completion, the water level in the small buckets was measured to calculate the volumes of runoff samples. After a 3 h settling period, 50 mL of the supernatant was taken and placed in a refrigerator at 0–4 °C for subsequent chemical analysis. After discarding a portion of the supernatant, the water–sediment mixture was dried and weighed to calculate the sediment content. The ammonium nitrogen concentration in the runoff was measured using a UV spectrophotometer.

After each rainfall event, the top 20 cm of soil was removed and backfilled with local topsoil. Settlement treatment was applied to the slope at a rainfall intensity of 20 mm h^{-1}, and after stabilization, the next round of rainfall was initiated. Each treatment was repeated three times.

2.4. Equations and Statistical Analysis

2.4.1. Soil Loss Rate and Ammonia Nitrogen Loss Rate

The soil loss rate refers to the mass of soil lost per unit area per unit time and can be calculated using the sediment content and runoff rate:

$$S_r = S_c \times R_r \tag{1}$$

where S_r refers to soil loss rate (g m^{-2} min^{-1}), S_c refers to sediment concentration (g L^{-1}), and R_r represents runoff rate (mm min^{-1}). The ammonia nitrogen loss rate represents the mass of ammonium nitrogen lost per unit area per unit time through runoff. It can be calculated using the ammonia nitrogen concentration and runoff rate:

$$N_r = N_c \times R_r \tag{2}$$

where N_r is the ammonia nitrogen loss rate (mg m^{-2} min^{-1}) and N_c is the ammonia nitrogen concentration in runoff.

2.4.2. Hydraulic Parameters

The flow velocity measured using a tracer is considered as the surface flow velocity. The average flow velocity can be calculated using the following formula:

$$v = kv_s \tag{3}$$

where v is the average velocity (m s^{-1}), v_s is the surface flow velocity (m s^{-1}), and k is the correlation coefficient, which is 0.67 for laminar flow (R_e < 500), 0.70 for transitional flow (500 < R_e < 2000), and 0.80 for turbulent flow (R_e > 2000).

The flow depth is a key parameter that reflects the hydrodynamic characteristics of the slope. However, it is hard to use traditional methods to accurately measure flow depth due to its very small value. In general, flow depth is derived through calculations involving the average flow velocity of runoff and unit discharge. For similarity, it is assumed that the slope runoff depth is uniformly distributed along the slope, and it can be expressed as follows:

$$h = \frac{q}{v} \tag{4}$$

where h is the flow depth (m) and q is the unit discharge (m^2 s^{-1}). The Reynolds number can be expressed as:

$$R_e = \frac{R_h v}{\mu} \tag{5}$$

where R_e is the Reynolds number and R_h is the hydraulic radius (m), which can be approximated as the flow depth when the flow depth is small. μ is kinematical viscosity (m^2 s^{-1}), which can be calculated using the following formula:

$$\mu = \frac{0.01775}{(1 + 0.0337\,T + 0.000221\,T^2)} \tag{6}$$

where T is the water temperature (°C). The Froude number for slope flow can be expressed as:

$$F_r = \frac{v}{\sqrt{gR_h}} \tag{7}$$

where F_r is the Froude number and g is the gravitational acceleration (m s^{-2}). The shear stress can be expressed as:

$$\tau = \rho g R_h J \tag{8}$$

where τ is the shear stress (Pa), ρ is the water density (kg m^{-3}), and J is the hydraulic gradient. The stream power can be expressed as:

$$\omega = \tau v \tag{9}$$

where ω is the stream power (N m^{-1} s^{-1}). The unit stream power can be expressed as:

$$P = vJ \tag{10}$$

where P is the unit stream power (m s^{-1}). The unit energy can be expressed as:

$$E = \frac{v^2}{2g} + h \tag{11}$$

where E is the unit energy of cross section (m), which is the sum of water potential energy and kinetic energy.

2.4.3. Statistical Analysis

The significance of the impacts of the slope gradient and rainfall intensity on flow hydraulic parameters was analyzed using SPSS 25.0 at the 0.05 significance level with the one-way analysis of variance. The correlation between the slope gradient, rainfall intensity and hydraulic parameters, soil loss rate, ammonia nitrogen loss rate; and the correlation between soil loss rate, ammonia nitrogen loss rate, and hydraulic parameters were all analyzed using SPSS 25.0 at the 0.01 significance level. The coefficient of determination (R^2) and root mean square error ($RMSE$) were applied to evaluate the performance of these correlations, which can be expressed as:

$$R^2 = \frac{\left[\sum_{i=1}^{n}(o_i - o_m)(p_i - p_m)\right]^2}{\sum_{i=1}^{n}(o_i - o_m)^2 \sum_{i=1}^{n}(p_i - p_m)^2} \tag{12}$$

$$RMSE = \sqrt{\frac{\sum_{i=1}^{n}(o_i - p_i)^2}{n}} \tag{13}$$

$$MAE = \frac{\sum_{i=1}^{n}|o_i - p_i|}{n} \tag{14}$$

$$MBE = \frac{\sum_{i=1}^{n}(p_i - o_i)}{n} \tag{15}$$

$$WIA = 1 - \frac{\sum_{i=1}^{n}(o_i - p_i)^2}{\sum_{i=1}^{n}(|p_i - o_m| + |o_i - o_m|)^2} \tag{16}$$

where n is the total number of the data points, o_i is the observed value at time i, o_m is the average observed value, p_i is the predicted value at time i, and p_m is the average predicted value.

3. Results

3.1. Flow Hydraulic Parameters

3.1.1. Flow Velocity and Flow Depth

The responses of the average flow velocity to the slope gradient and rainfall intensity were shown in Figure 2a. Under a rainfall intensity of 75 mm h^{-1}, the runoff velocities for slopes of 8.7%, 17.6%, 26.8%, and 36.4% were 0.114 m s^{-1}, 0.156 m s^{-1}, 0.173 m s^{-1}, and 0.188 m s^{-1}, respectively. The results indicated that the overland flow velocity increased with the slope, and similar trends were observed at other rainfall intensities. The analysis of variance revealed that under a rainfall intensity of 75 mm h^{-1}, the flow velocity significantly increased with an increase in the slope gradient ($p < 0.05$). At 50 mm h^{-1}, only the flow velocities on 17.6% and 26.8% slopes did not exhibit significant differences. However, at a rainfall intensity of 25 mm h^{-1}, except for the 36.4% slope where the velocity was significantly greater than that of the 8.7% slope, there were no significant differences in the other groups. This suggested that an increasing flow velocity with an increase in the slope gradient may be influenced by the rainfall intensity. Additionally, the flow velocity also showed significant increases with an increase in the rainfall intensity ($p < 0.05$). According to that, the flow velocity change with the slope gradient and rainfall intensity can be described as follows:

$$v = 0.013r^{0.691}G^{0.306}(R^2 = 0.979, n = 12, RMSE = 0.007) \tag{17}$$

where r is the rainfall intensity (mm h^{-1}) and G is the slope gradient (%). The fitting results indicated that the flow velocity, rainfall intensity, and slope gradient were highly

(R^2 = 0.979) and significantly ($p < 0.01$) related. The rainfall intensity and slope gradient were good predictors of overland flow velocity, with the *MAE*, *MBE*, and *WIA* being 0.0047, −0.0001 and 0.995 (Table 2).

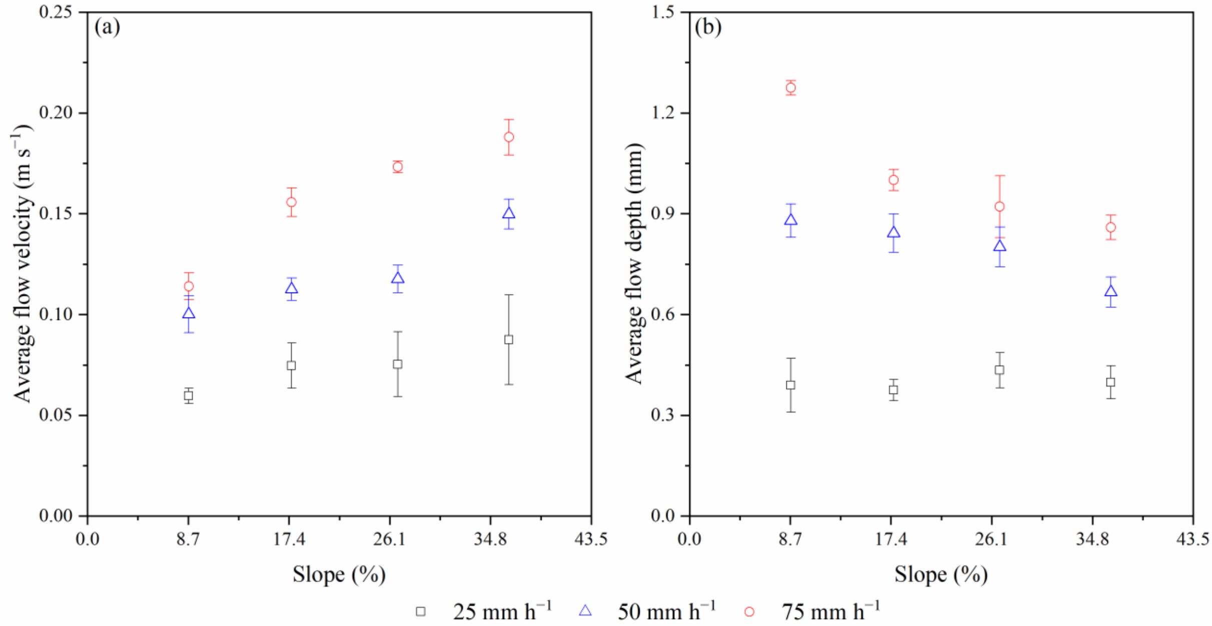

Figure 2. Responses of average flow velocity and flow depth to the slope gradient and rainfall intensity: (**a**) flow velocity; (**b**) flow depth.

Table 2. Fitting statistical indicators of R^2, *MAE*, *MBE* and *WIA* between the observed and predicted flow velocity, flow depth, shear stress, stream power, unit stream power, unit energy, soil loss rate, and ammonia nitrogen loss rate based on the slope gradient and rainfall intensity.

Predicted Parameter	R^2	*MAE*	*MBE*	*WIA*
Flow velocity	0.979	0.0047	−0.0001	0.995
Flow depth	0.949	0.1877	−0.1877	0.962
Shear stress	0.981	0.0828	0.0111	0.995
Stream power	0.997	0.0076	0.0003	0.999
Unit stream power	0.995	0.0012	0.0007	0.998
Unit energy	0.993	0.0000	0.0000	0.998
Soil loss rate	0.990	4.4293	0.7808	0.997
Ammonia nitrogen loss rate	0.984	0.1052	−0.0443	0.996

With an increase in the slope gradient, the overall trend of flow depth generally decreased. For instance, at a rainfall intensity of 75 mm h^{-1}, the average flow depth of an 8.7% slope was 1.27 mm, which was 1.27, 1.38, and 1.48 times the flow depths at slopes of 17.6%, 26.8%, and 36.4%, respectively (Figure 2b). Under rainfall intensities of 75 and 50mm h^{-1}, the flow depth tended to significantly decrease with an increase in the slope gradient ($p < 0.05$). However, at a rainfall intensity of 25 mm h^{-1}, the flow depths were 0.390 mm and 0.399 mm for 8.7% and 36.4% slopes, respectively, indicating that there was not an evident change in the water depth with an increasing slope. Thus, the relationship between ground slope and flow depth varied with changes in the rainfall intensity. On an 8.7% slope, the flow depths were 0.389 mm and 1.275 mm under rainfall intensities of 25 and 75 mm h^{-1}, suggesting a significant increase with an increase in the rainfall intensity ($p < 0.05$). Therefore, the relationship between flow depth, slope gradient, and rainfall intensity was established as follows:

$$h = 0.022r^{0.817}G^{-0.212}(R^2 = 0.949, n = 12, RMSE = 0.072) \tag{18}$$

The fitting results indicated that the flow depth, rainfall intensity, and slope gradient were highly (R^2 = 0.979) and significantly (p < 0.01) related. The rainfall intensity and slope gradient were good predictors of flow depth, with the *MAE*, *MBE*, and *WIA* being 0.1877, −0.1877 and 0.962 (Table 2).

3.1.2. Flow Regime

The Reynolds number ranged from 20.57 to 141.69 (Figure 3a), indicating that the overland flow was laminar under all treatments of rainfall intensity and slope gradient. At a rainfall intensity of 25 mm h^{-1}, the Reynolds number ranged from 20.57 to 29.97. This suggested that under the same rainfall intensity conditions, there was not a significant change in the Reynolds number with an increasing slope, which could be also found under rainfall intensities of 75 and 50 mm h^{-1}. The Reynolds numbers were 20.57, 77.26, and 127.47 under rainfall intensities of 25, 50, and 75 mm h^{-1} on an 8.7% slope, respectively, indicating an increase with the increase in rainfall intensity.

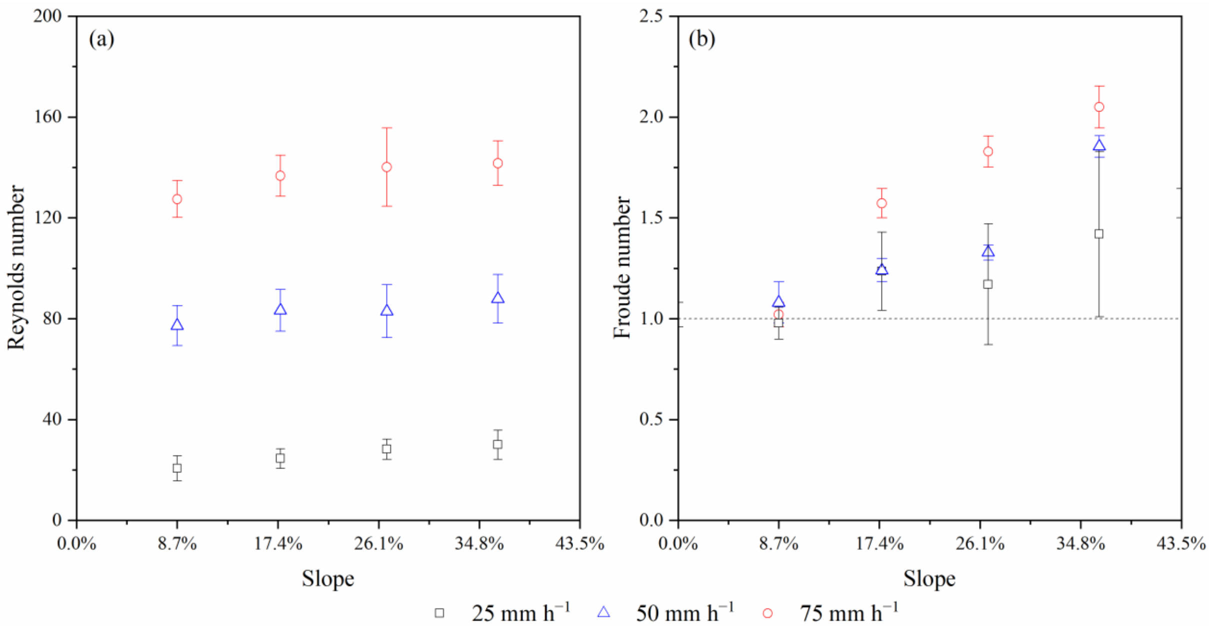

Figure 3. Responses of Reynolds number and Froude number to the slope gradient and rainfall intensity, (**a**): Reynolds number; (**b**): Froude number.

The Froude number was found to increase with an increase in the slope gradient (Figure 3b). The Froude numbers were 1.02, 1.57, 1.83, and 2.05 for 8.7%, 17.6%, 26.8%, and 36.4% slopes under a rainfall intensity of 75 mm h^{-1}. Under the conditions of a 25 mm h^{-1} rainfall intensity and an 8.7% slope gradient, the Froude number was 0.98, which is less than 1, indicating that the overland flow was subcritical flow. In the remaining treatments, the Froude number was greater than 1, indicating that the overland flow of these treatments was supercritical flow. The Froude number also increased with an increase in the rainfall intensity, and the magnitude of increase grew with the increase in slope.

3.1.3. Shear Stress, Stream Power, Unit Stream Power, and Unit Energy

The shear stress ranged from 0.33 to 1.09, 0.65 to 1.73, 1.14 to 2.42, and 1.42 to 3.06 Pa, respectively, under slope gradients of 8.7%, 17.6%, 26.8%, and 36.4% (Figure 4a). The results indicated that shear stress significantly increased with an increase in the slope gradient (p < 0.05). Additionally, shear stress also significantly increased with an increase in the rainfall intensity (p < 0.05). Therefore, the shear stress can be predicted using the product of rainfall intensity and slope power function, as shown in the following equation:

$$\tau = 0.326 r^{0.707} G^{0.778} (R^2 = 0.981, n = 12, RMSE = 0.125) \quad (19)$$

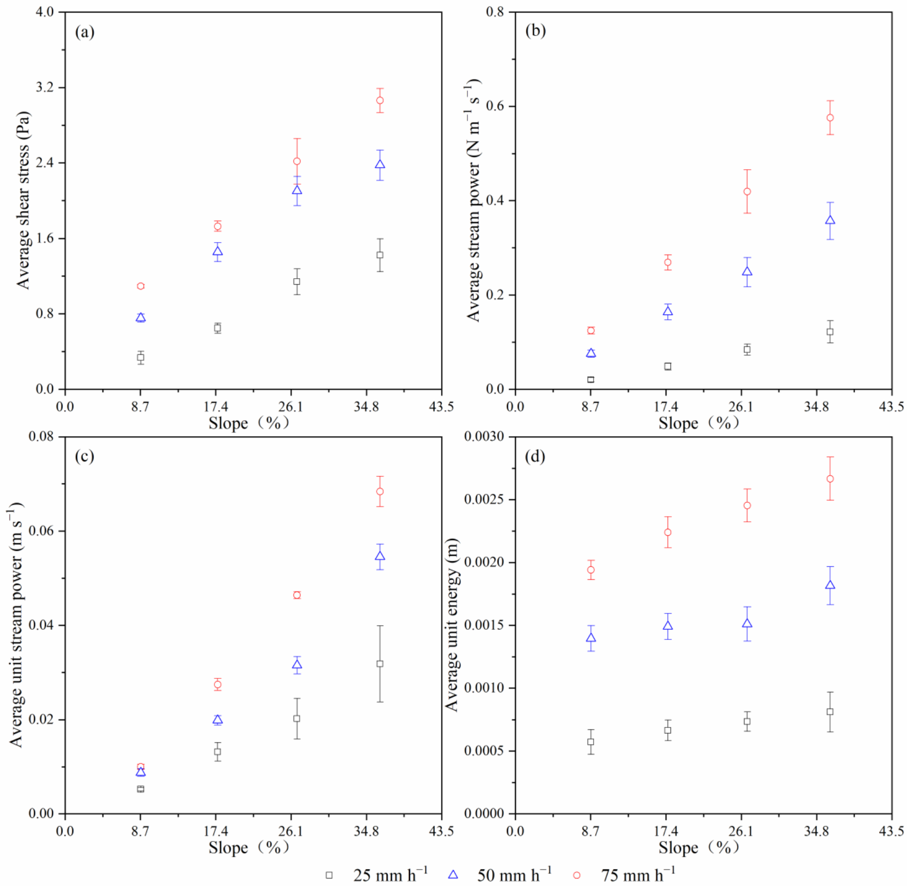

Figure 4. Responses of average shear stress, stream power, unit stream power, and unit energy to the slope gradient and rainfall intensity: (**a**) shear stress; (**b**) stream power; (**c**) unit stream power; (**d**) unit energy.

The equation indicated that the shear stress, rainfall intensity, and slope gradient were highly and significantly ($p < 0.01$) related. The rainfall intensity and slope gradient were good predictors of shear stress (*RMSE* = 0.125).

The average stream power of a 36.4% slope was 0.576 N m^{-1} s^{-1}, which was 4.62, 2.14, and 1.37 times of those of 8.7%, 17.6%, 26.8% treatments under 75 mm h^{-1} (Figure 4b), respectively, showing a significant increase with an increase in the slope gradient ($p < 0.05$). There was a similar trend in other rainfall intensities. The relationship between slope gradient and stream power varied with changes in the rainfall intensity. The increasing speed of stream power was notably faster at a rainfall intensity of 75 mm h^{-1} compared to the other two rainfall intensities. Moreover, the average stream power significantly increased with an increase in the rainfall intensity ($p < 0.05$). The relationships between average stream power, rainfall intensity, and slope gradient could also be expressed as the product of the rainfall intensity and slope power function:

$$\omega = 0.005r^{1.353}G^{1.074}(R^2 = 0.997, n = 12, RMSE = 0.011) \tag{20}$$

The patterns of change in the average unit stream power and unit energy with the slope gradient were similar to those of average stream power and shear stress, with an increase when the slope gradient increased (Figure 4c,d). The average unit stream power significantly increased with the increase in slope under the same rainfall intensity ($p < 0.05$). However, in terms of average unit energy, there was generally no significant difference in the average unit energy among different slopes under rainfall intensities of 50 and 25 mm h^{-1}. Additionally, the average unit stream power and unit energy significantly increased with an increase in the rainfall intensity ($p < 0.05$). The relationships between unit stream power, unit energy, rainfall intensity, and slope gradient could also be expressed as follows:

$$P = 0.013r^{0.705}G^{1.329}(R^2 = 0.995, n = 12, RMSE = 0.002) \quad (21)$$

$$E = 3.215 \times 10^{-5}r^{1.07}G^{0.209}(R^2 = 0.993, n = 12, RMSE = 6.78 \times 10^{-5}) \quad (22)$$

3.1.4. Soil Loss Rate and Ammonia Nitrogen Loss Rate

The average soil loss rate and total soil loss increased with an increase in the slope gradient under the same rainfall conditions ($p < 0.05$). In instances of high rainfall intensity and steep slopes, there were notable fluctuations in the soil loss rates (Figure 5). This phenomenon may be attributed to the smoothing of the soil surface, nonuniform infiltration on the slope, and limited connectivity of flow. With the generation of runoff, a portion of the surface soil on the slope is carried away, resulting in a reduction in surface roughness and a smoothing of the slope. This protects the soil from erosion but simultaneously reduces the resistance to overland flow on the slope, increasing kinetic energy and consequently raising the sediment transport rate [24–26]. Nonuniform infiltration on the slope can impact the formation of continuous overland flow, similarly leading to fluctuations in sediment transport rates [27]. The results showed that the soil erosion rate significantly increased with an increase in the rainfall intensity ($p < 0.05$). For instance, the average soil erosion rate was 188.56 g m^{-2} min^{-1} at a 36.4% slope, which was 146.70 g m^{-2} min^{-1} larger than that of an 8.7% slope treatment under a 75 mm h^{-1} rainfall intensity. Therefore, the relationships between average soil loss rate, rainfall intensity, and slope gradient could also be expressed as follows:

$$S_r = 0.095r^{2.06}G^{1.28}(R^2 = 0.990, n = 12, RMSE = 6.46) \quad (23)$$

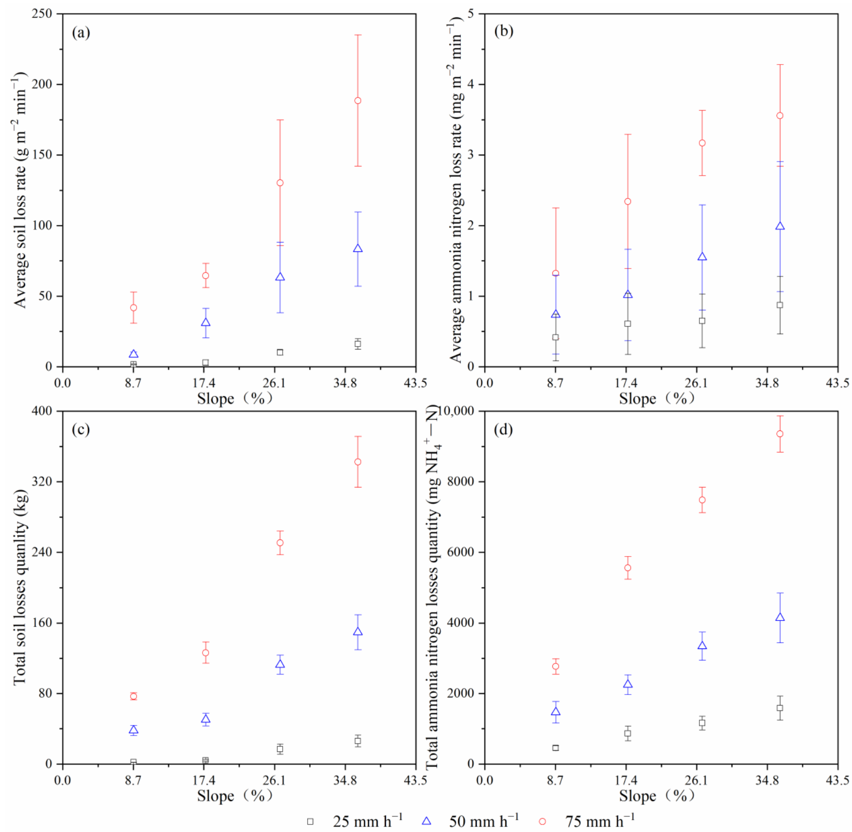

Figure 5. Responses of soil loss rate and ammonia nitrogen loss rate to the slope gradient and rainfall intensity: (**a**) soil loss rate; (**b**) ammonia nitrogen loss rate; (**c**) total sediment losses; (**d**) total ammonia losses.

The average ammonia loss rate and total ammonia loss quantity exhibited a significant rise with an increase in the slope gradient under the same rainfall conditions ($p < 0.05$). There was a noticeable fluctuation in the ammonia nitrogen loss rate (Figure 5). This may be attributed to the continuous decrease in nutrient concentration in the runoff. Furthermore, the results indicated a substantial increase in the average ammonia nitrogen loss rate and total ammonia nitrogen loss with a rise in the rainfall intensity ($p < 0.05$). For instance, at a slope of 36.4%, the average ammonia loss rate was 3.56 mg m^{-2} min^{-1}, which was 2.24 mg m^{-2} min^{-1} higher than that observed in the 8.7% slope treatment under a 75 mm h^{-1} rainfall intensity. Consequently, the relationships between average ammonia nitrogen loss rate, rainfall intensity, as well as slope gradient could be expressed as follows:

$$N_r = 0.014r^{1.44}G^{0.67}(R^2 = 0.984, n = 12, RMSE = 0.145) \quad (24)$$

3.1.5. Relationship between Hydraulic Parameters, Soil Erosion Rate, and Ammonia Nitrogen Loss Rate

An analysis was conducted on the influence of shear stress, hydraulic power, unit hydraulic power, and unit energy on soil erosion rates, as well as the impact of their respective averages on the average soil erosion rate (Figure 6). The results indicated that soil erosion rates could be described by the power function of shear stress, hydraulic power, unit hydraulic power, and unit energy, with the R^2, *MAE*, *MBE*, and *WIA* ranging from 0.748 to 0.909, 12.024 to 22.2258, −2.648 to −0.289, and 0.926 to 0.976, respectively (Table 3). Similarly, the average soil erosion rate also showed a power relationship with the average shear stress, hydraulic power, unit hydraulic power, and unit energy, with the R^2, *MAE*, *MBE*, and *WIA* ranging from 0.823 to 0.980, 5.430 to 18.788, −2.490 to 0.043, and 0.951 to 0.995, respectively. This suggested that the hydraulic parameters were good indicators of either average or process soil erosion rates. For both the average values and process values, the fitting performance of stream power was optimal (R^2 = 0.980 and 0.909, respectively), indicating that stream power could serve as a characteristic parameter for predicting soil erosion rates. It could also be concluded that the coefficients of the average values were smaller than those of process values. For instance, the equation coefficients of the average shear stress were 13.4 and 2.359, respectively, which were smaller than those of the process values, namely, 13.7 and 2.328, respectively.

Table 3. Fitting statistical indicators of R^2, *MAE*, *MBE* and *WIA* between the observed and predicted process soil loss rate and average soil loss rate based on the shear stress, stream power, unit stream power, and unit energy.

Predicted Parameter	Hydraulic Parameter	R^2	*MAE*	*MBE*	*WIA*
Average soil loss rate	Average shear stress	0.937	10.596	−0.576	0.984
	Average stream power	0.980	5.430	0.043	0.995
	Average unit stream power	0.823	18.788	−1.369	0.951
	Average unit energy	0.875	14.786	−2.490	0.967
Soil loss rate	Shear stress	0.844	16.070	−0.670	0.957
	Stream power	0.909	12.024	−0.289	0.976
	Unit stream power	0.748	22.258	−1.969	0.926
	Unit energy	0.831	18.470	−2.648	0.954

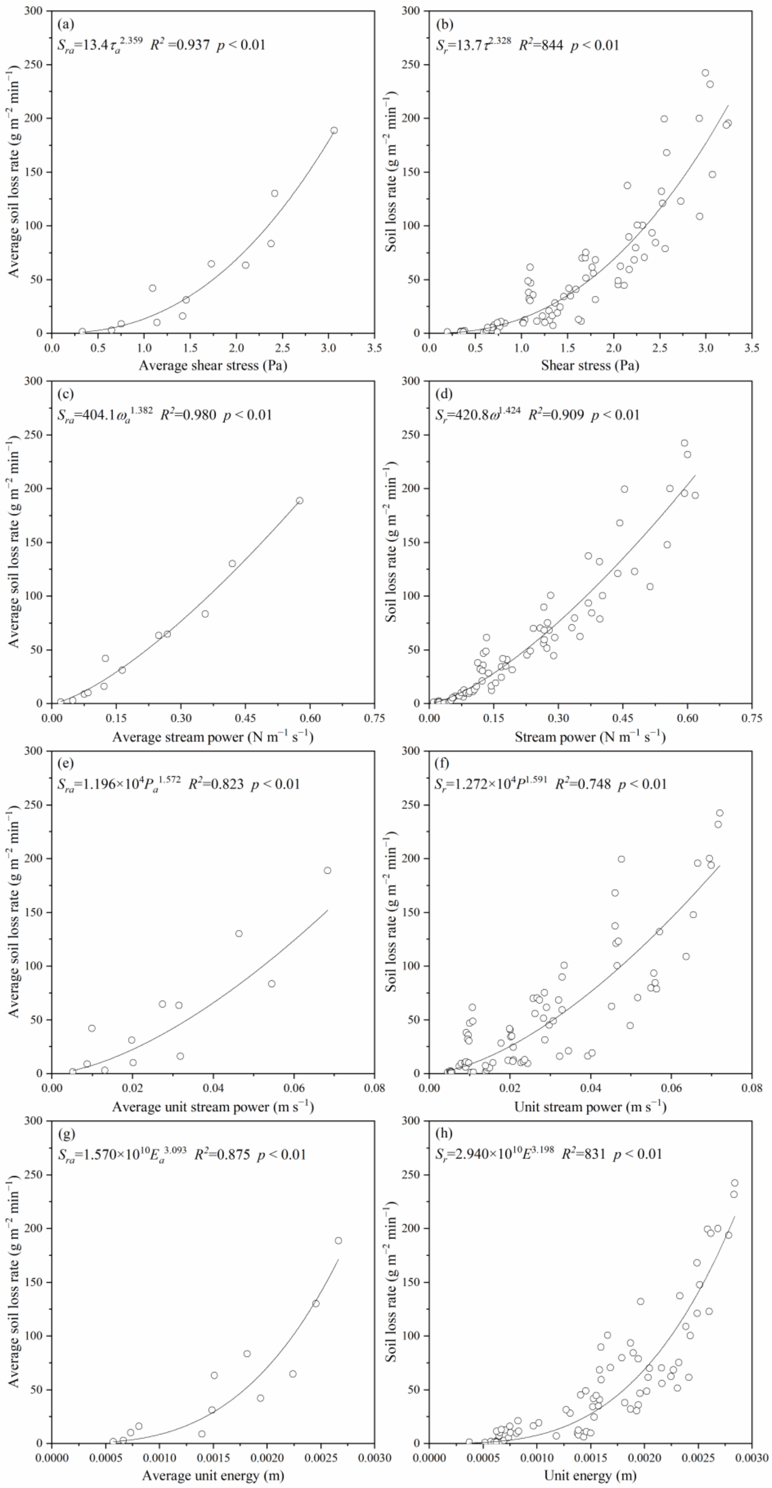

Figure 6. Average soil loss rate and soil loss rate as a function of the flow hydraulic parameters: (**a**,**b**) shear stress; (**c**,**d**) stream power; (**e**,**f**) unit stream power; (**g**,**h**) unit energy.

In contrast to the relationships between hydraulic parameters and soil loss rates, the ammonia nitrogen loss rate showed a linear increasing trend with the increase in shear stress, hydraulic power, unit hydraulic power, and unit energy (Figure 7). For the average ammonia nitrogen loss rate, the R^2, *MAE*, *MBE*, and *WIA* ranged between 0.714 and 0.933, 0.2070 and 0.4374, −0.0023 and 0.0002, and 0.910 and 0.982, respectively (Table 4), while for the process value, the R^2, *MAE*, *MBE*, and *WIA* ranged between 0.450 and 0.587, 0.6071 and 0.6966, −0.0012 and 0.0005, and 0.785 and 0.857, respectively. The results indicated that the hydraulic parameters were good indicators of the average ammonia nitrogen loss rate, and the best predictor was the stream power. However, the hydraulic parameters may not be appropriate to predict the process values.

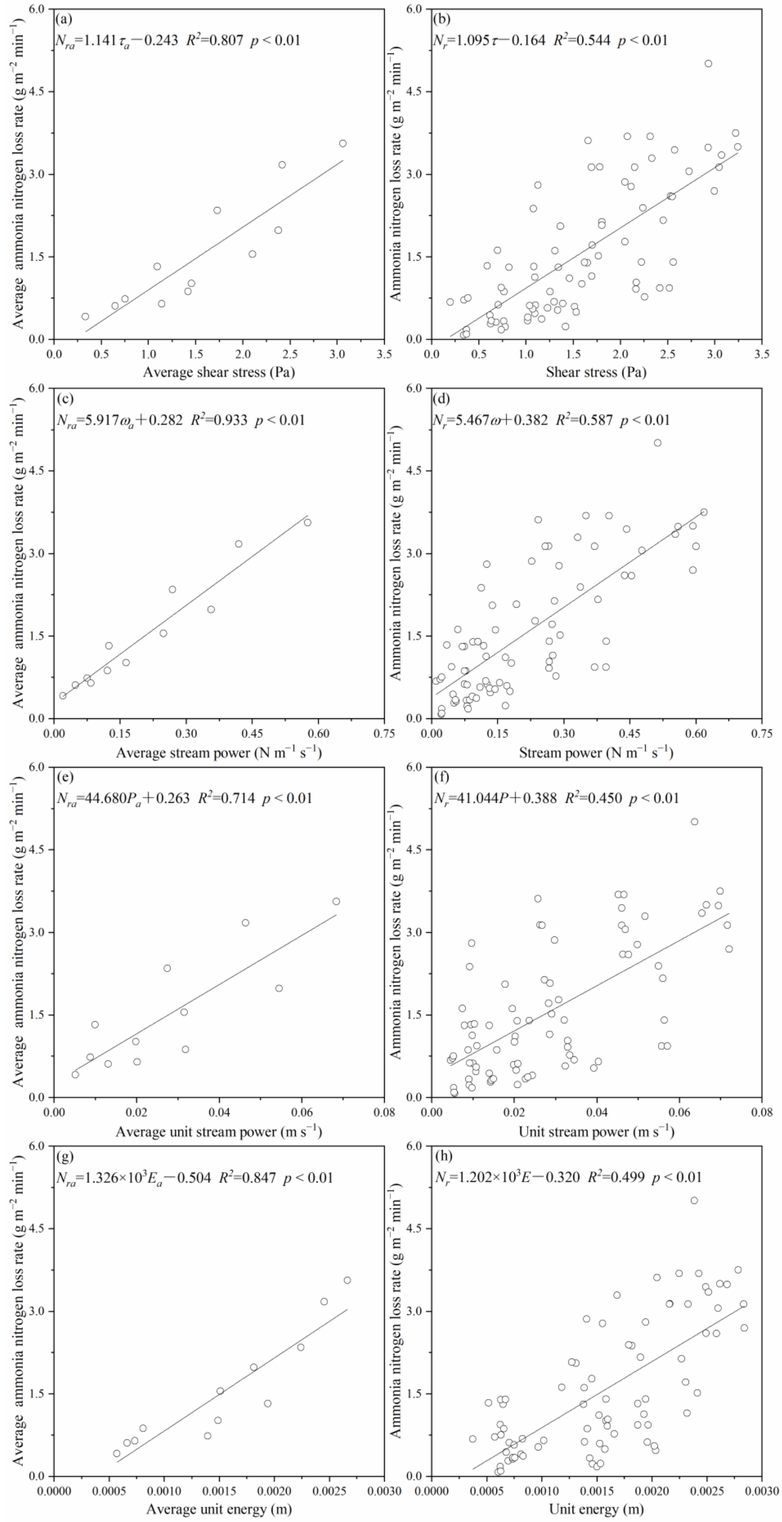

Figure 7. Average ammonia nitrogen loss rate and ammonia nitrogen loss rate as a function of the flow hydraulic parameters: (**a**,**b**) shear stress; (**c**,**d**) stream power; (**e**,**f**) unit stream power; (**g**,**h**) unit energy.

Table 4. Fitting statistical indicators of R^2, *MAE*, *MBE*, *WIA*, and *WIA* between the observed and predicted process ammonia nitrogen loss rate and average ammonia nitrogen loss rate based on the shear stress, stream power, unit stream power, and unit energy.

Predicted Parameter	Hydraulic Parameter	R^2	*MAE*	*MBE*	*WIA*
Average ammonia nitrogen loss rate	Average shear stress	0.807	0.4009	0.0004	0.944
	Average stream power	0.933	0.2070	0.0002	0.982
	Average unit stream power	0.714	0.4374	0.0002	0.910
	Average unit energy	0.847	0.3238	−0.0023	0.958
Ammonia nitrogen loss rate	Shear stress	0.544	0.6201	0.0003	0.836
	Stream power	0.587	0.6071	0.0004	0.857
	Unit stream power	0.450	0.6966	0.0005	0.785
	Unit energy	0.499	0.6868	−0.0012	0.809

4. Discussion

4.1. Impact of Slope Gradient and Rainfall Intensity on Flow Hydraulic Parameters

Overland flow encounters resistance along the upslope direction and gravitational forces along the downslope direction. With an increase in the slope, the gravitational force component grows, leading to an enhanced downslope flow velocity [28,29] (Figure 2). This observation aligns with the prior study's findings [29]. However, as depicted in Figure 2, under a low rainfall intensity, the change in the slope flow velocity with an increasing slope is negligible. This may be attributed to the smaller runoff volume and relatively lower flow velocity values associated with a low rainfall intensity. Simultaneously, the resistance on the slope is higher, resulting in a uniform or decelerated flow along the slope. In such scenarios, the impact of the slope on the runoff velocity is minimal [28,30,31]. The runoff velocity is directly proportional to the product of the power function of slope and the power function of rainfall intensity, consistent with earlier research findings [32]. Equation (4) indicates that the slope flow depth is primarily influenced by flow velocity and unit discharge. As the slope increases, the unit discharge also rises. As discussed earlier, the runoff velocity also experiences an increase. For rainfall intensities of 75 and 50 mm h^{-1}, the runoff depth decreases with an increasing slope, likely due to the predominant effect of an increased flow velocity with slope. This is in accordance with previous findings [33]. However, when the rainfall intensity is 25 mm h^{-1}, the variation in flow depth is not significant. This might be attributed to the minimal changes in the flow velocity and unit discharge with slope under low rainfall intensity conditions. Under the same slope conditions, the rainfall intensity significantly increases the runoff volume, consequently leading to a higher runoff velocity and water depth [23,34].

Shear stress, stream power, unit stream power, and unit energy also increased with the slope gradient and rainfall intensity. According to Equation (8), it can be inferred that shear stress is primarily associated with the hydraulic gradient and hydraulic radius. The hydraulic gradient of runoff increases with the increase in slope, while the hydraulic radius gradually decreases with the increase in slope (Figure 2b). This indicates that the hydraulic gradient has a major impact on shear stress. This relationship can also be derived through Equation (17), where the coefficient G is -0.212; multiplying this by the hydraulic gradient gives the coefficient of G in the shear stress fitting equation as 0.778. Similarly, the stream power, unit stream power, and unit energy can all be expressed as functions of the flow velocity, water depth, and hydraulic gradient, which are all positively correlated with the slope. Considering the relationships between the hydraulic parameters, rainfall intensity, and slope, it is noted that the stream power has the fastest growth rate with an increasing rainfall intensity, followed by unit energy, shear stress, and unit stream power. Meanwhile, with an increasing slope, the fastest growth rate is observed for unit stream power, followed by stream power, shear stress, and unit energy.

4.2. Impact of Slope Gradient and Rainfall Intensity on Soil and Ammonia Nitrogen Loss

The increase in slope enhances the flow velocity, facilitating easier water movement and augmenting the kinetic energy of the flow, leading to a stronger shear stress and stream power, prompting the movement of soil particles [35]. Simultaneously, the heightened slope increases the gravitational force along the slope, amplifying the impact force of water flow, resulting in more substantial erosive effects on the soil surface. An increasing slope also results in an elevated nutrient loss rate. This is primarily attributed to the reduction in slope surface infiltration and the subsequent increase in runoff [11,22], thereby amplifying the carrier for nutrient transport [36]. Additionally, the increase in slope enhances the surface flow velocity, leading to an escalated erosive force and turbulence in the runoff [20,23]. This heightened flow velocity increases the possibility of nutrients from the soil entering the runoff and being carried away by it [37].

With the rise in rainfall intensity, more runoff is generated, increasing the erosive capability of overland flow as the larger runoff carries away more soil particles [24,38,39]. Furthermore, the heightened rainfall intensity induces more intense raindrop impact, with larger raindrops striking the soil surface at higher speeds, causing more soil erosion and accelerating the processes of soil loss. Generally, a higher rainfall intensity is associated with lower nutrient concentrations in the runoff. This is primarily because a greater rainfall intensity implies a larger volume of runoff, typically resulting in the dilution of nutrient concentrations [40]. Additionally, it is worth noting that a higher rainfall intensity usually corresponds to larger products of runoff rate and nutrient concentration, aligning with our research findings [41].

4.3. The Relationship between Soil Loss, Ammonia Nitrogen Loss and Hydraulic Parameters

Our research indicates that the soil erosion rate follows a power function growth with hydraulic parameters, which is consistent with the earlier research findings [15,16]. However, some studies suggest that sediment loss increases exponentially with shear stress, while others show power or linear trends. Section 4.1 highlighted the inconsistencies in the rates at which hydraulic parameters increase with the rainfall intensity and slope. As the slope increases from sheet erosion to the formation of rill erosion, the soil erosion rate undergoes significant changes, showing exponential or power function growth trends. However, when only sheet erosion or interrill erosion occurs, the soil loss rate changes more steadily, and a linear function may be more appropriate. Our study demonstrates that hydraulic parameters can effectively fit the average soil loss rate and process soil erosion rate, with the R^2, *MAE*, *MBE*, and *WIA* ranging from 0.748 to 0.980, 5.430 to 22.258, -2.490 to 0.043, and 0.926 to 0.995, respectively, indicating that hydraulic parameters can act as characteristic parameters for soil erosion rates. For both the average soil erosion rate and process soil erosion rate, stream power emerges as the optimal parameter, with an R^2 of 0.980 and 0.909, respectively. Coefficients for the average soil erosion rate and process soil erosion rate differ, with the constant and exponent for average soil erosion rate being smaller compared to process quantities. This may be attributed to averaging the mitigating peak soil erosion rates.

For the ammonia nitrogen loss rate, hydraulic parameters exhibit a good linear relationship with the average ammonium nitrogen loss rate, with the R^2, *MAE*, *MBE*, and *WIA* ranging from 0.714 to 0.933, 0.207 to 0.437, -0.002 to 0.0002, and 0.910 to 0.982, respectively, but this linear relationship has a relatively lower R^2 in the process quantities. This may be caused by the fact that the ammonia nitrogen concentration gradually decreases over time, reaching a stable rate more slowly than hydraulic parameters [42]. This can lead to situations where hydraulic parameters show minimal change, but the ammonia nitrogen loss rate varies significantly, resulting in a more dispersed relationship. However, as analyzed earlier, the overall trend is that ammonia nitrogen loss rates increase with the slope gradient and rainfall intensity, which aligns with the changes in hydraulic parameters. Thus, hydraulic parameters can be utilized as characteristic indicators for representing average nutrient loss rates or the total amount of nutrient loss but may not be suitable for fitting process quantities.

5. Conclusions

In this study, we conducted simulated rainfall experiments to explore variations in flow hydraulic parameters, soil loss, and ammonia nitrogen loss processes under different slope gradients and rainfall intensities. Our results showed that under the same rainfall intensity, the flow velocity, shear stress, stream power, unit stream power, unit energy increased, average soil loss rate, and average ammonia nitrogen loss rate increased with the slope gradient, but flow depth decreased with the slope gradient. Given the same slope gradient, the hydraulic parameters, average soil loss rate, and average ammonia nitrogen loss rate all increased with the slope gradient. Furthermore, the hydraulic parameters, average soil loss rate, and average ammonia nitrogen loss rate could be described by the product of slope gradient and rainfall intensity power function. Stream power was found to be the best hydraulic predictor for estimating both the average soil loss rate and process soil loss rate (R^2 = 0.980 and 0.909, respectively). The stream power could be used to predict the average ammonia nitrogen loss rate but may not be appropriate to predict the process ammonia nitrogen loss rate. Our results underscore the significant impacts of the slope gradient and rainfall intensity on the slope hydraulic parameters, and they advocate for the integration of flow hydraulic parameters in the development of models for predicting soil loss and nutrient loss.

Author Contributions: W.X. designed the experiment; H.Y., C.W., G.S. and X.T. conducted the experiment; H.Y. and G.S. wrote the manuscript; C.W. provided laboratory and other technical support; W.X. and Y.W. critically reviewed and edited the manuscript. All authors have read and agreed to the published version of the manuscript.

Funding: This study received funding from the Natural Science Foundation of Jiangsu Province, China (grant Nos. BK20200955 and BK20210824); National Natural Science Foundation of China (grant No. 52009117); and Knowledge Innovation Program of Wuhan–Shuguang Project (grant No. 2023020201020362).

Data Availability Statement: Data are contained within the article.

Acknowledgments: We appreciate and thank the anonymous reviewers for their helpful comments that led to an overall improvement of the manuscript. We also thank the journal's editor board for their help and patience throughout the review process.

Conflicts of Interest: The authors declare no conflict of interest.

References

1. Borrelli, P.; Robinson, D.A.; Fleischer, L.R.; Lugato, E.; Ballabio, C.; Alewell, C.; Meusburger, K.; Modugno, S.; Schütt, B.; Ferro, V.; et al. An assessment of the global impact of 21st century land use change on soil erosion. *Nat. Commun.* **2017**, *8*, 2013. [CrossRef]
2. Giménez-Morera, A.; Sinoga, J.D.R.; Cerdà, A. The impact of cotton geotextiles on soil and water losses from Mediterranean rainfed agricultural land. *Land Degrad. Dev.* **2010**, *21*, 210–217. [CrossRef]
3. Govindaraju, R.S.; Kavvas, M.L. Modeling the erosion process over steep slopes: Approximate analytical solutions. *J. Hydrol.* **1991**, *127*, 279–305. [CrossRef]
4. Zhang, X.C.; Nearing, M.A.; Norton, L.D.; Miller, W.P.; West, L.T. Modeling Interrill Sediment Delivery. *Soil Sci. Soc. Am. J.* **1998**, *62*, 438–444. [CrossRef]
5. Nearing, M.A.; Norton, L.D.; Bulgakov, D.A.; Larionov, G.A.; West, L.T.; Dontsova, K.M. Hydraulics and erosion in eroding rills. *Water Resour. Res.* **1997**, *33*, 865–876. [CrossRef]
6. Nearing, M.A.; Foster, G.R.; Lane, L.J.; Finkner, S.C. A Process-Based Soil Erosion Model for USDA-Water Erosion Prediction Project Technology. *Trans. ASAE* **1989**, *32*, 1587–1593. [CrossRef]
7. Deelstra, J.; Iital, A.; Povilaitis, A.; Kyllmar, K.; Greipsland, I.; Blicher-Mathiesen, G.; Jansons, V.; Koskiaho, J.; Lagzdins, A. Reprint of "Hydrological pathways and nitrogen runoff in agricultural dominated catchments in Nordic and Baltic countries". *Agric. Ecosyst. Environ.* **2014**, *198*, 65–73. [CrossRef]
8. Li, X.; Fu, S.; Liu, B. Response of flow hydraulic parameters to different rock fragment coverages and sizes under simulated rainfall. *Soil Tillage Res.* **2023**, *230*, 105707. [CrossRef]

9. Chen, B.; Zhang, X. Effects of slope vegetation patterns on erosion sediment yield and hydraulic parameters in slope-gully system. *Ecol. Indic.* **2022**, *145*, 109723. [CrossRef]
10. Jomaa, S.; Barry, D.A.; Heng, B.C.P.; Brovelli, A.; Sander, G.C.; Parlange, J.Y. Effect of antecedent conditions and fixed rock fragment coverage on soil erosion dynamics through multiple rainfall events. *J. Hydrol.* **2013**, *484*, 115–127. [CrossRef]
11. Peng, L.; Zhan-bin, L.; Liang-yong, Z. Hydrodynamics process of soil erosion and sediment yield by runoff on loess slope. *Adv. Water Sci.* **2006**, *17*, 444–449. (In Chinese with English Abstract)
12. Polyakov, V.O.; Nearing, M.A. Sediment transport in rill flow under deposition and detachment conditions. *CATENA* **2003**, *51*, 33–43. [CrossRef]
13. Mahmoodabadi, M.; Ghadiri, H.; Yu, B.; Rose, C. Morpho-dynamic quantification of flow-driven rill erosion parameters based on physical principles. *J. Hydrol.* **2014**, *514*, 328–336. [CrossRef]
14. Wu, B.; Wang, Z.; Zhang, Q.; Shen, N.; Liu, J. Modelling sheet erosion on steep slopes in the loess region of China. *J. Hydrol.* **2017**, *553*, 549–558. [CrossRef]
15. Wang, D.; Wang, Z.; Zhang, Q.; Zhang, Q.; Tian, N.; Liu, J.e. Sheet erosion rates and erosion control on steep rangelands in loess regions. *Earth Surf. Process. Landf.* **2018**, *43*, 2926–2934. [CrossRef]
16. Wang, C.; Wang, B.; Wang, Y.; Wang, Y.; Zhang, W. Improved interrill erosion prediction by considering the impact of the near-surface hydraulic gradient. *Soil Tillage Res.* **2020**, *203*, 104687. [CrossRef]
17. Wang, Y.; Luo, J.; Zheng, Z.; Li, T.; He, S.; Zhang, X.; Wang, Y.; Liu, T. Assessing the contribution of the sediment content and hydraulics parameters to the soil detachment rate using a flume scouring experiment. *CATENA* **2019**, *176*, 315–323. [CrossRef]
18. Li, G.; Zheng, F.; Lu, J.; Xu, X.; Hu, W.; Han, Y. Inflow Rate Impact on Hillslope Erosion Processes and Flow Hydrodynamics. *Soil Sci. Soc. Am. J.* **2016**, *80*, 711–719. [CrossRef]
19. Wu, B.; Li, L.; Xu, L.; Li, X. Modelling sheet erosion on steep slopes of clay loess soil using a rainfall simulator. *Biosyst. Eng.* **2022**, *216*, 1–12. [CrossRef]
20. Guo, T.; Wang, Q.; Li, D.; Zhuang, J.; Wu, L. Flow hydraulic characteristic effect on sediment and solute transport on slope erosion. *CATENA* **2013**, *107*, 145–153. [CrossRef]
21. Zhao, L.; Qin, Q.; Geng, H.; Zheng, F.; Zhang, X.J.; Li, G.; Xu, X.; Zhang, J. Effects of upslope inflow rate, tillage depth, and slope gradients on hillslope erosion processes and hydrodynamic mechanisms. *CATENA* **2023**, *228*, 107189. [CrossRef]
22. Gong, T.; Zhu, Y.; Shao, M.a. Effect of embedded-rock fragments on slope soil erosion during rainfall events under simulated laboratory conditions. *J. Hydrol.* **2018**, *563*, 811–817. [CrossRef]
23. Shen, H.; Zheng, F.; Wen, L.; Han, Y.; Hu, W. Impacts of rainfall intensity and slope gradient on rill erosion processes at loessial hillslope. *Soil Tillage Res.* **2016**, *155*, 429–436. [CrossRef]
24. Zhao, X.; Song, X.; Li, L.; Wang, D.; Meng, P.; Li, H. Effect of microrelief features of tillage methods under different rainfall intensities on runoff and soil erosion in slopes. *Int. Soil Water Conserv. Res.* **2023**. [CrossRef]
25. Gómez, J.; Nearing, M. Runoff and sediment losses from rough and smooth soil surfaces in a laboratory experiment. *CATENA* **2005**, *59*, 253–266. [CrossRef]
26. Schmaltz, E.M.; Johannsen, L.L.; Thorsøe, M.H.; Tähtikarhu, M.; Räsänen, T.A.; Darboux, F.; Strauss, P. Connectivity elements and mitigation measures in policy-relevant soil erosion models: A survey across Europe. *CATENA* **2024**, *234*, 107600. [CrossRef]
27. Chen, R.; Li, H.; Wang, J.; Song, Z. Critical factors influencing soil runoff and erosion in sprinkler irrigation: Water application rate and droplet kinetic energy. *Agric. Water Manag.* **2023**, *283*, 108299. [CrossRef]
28. Ban, Y.Y.; Wang, W.; Lei, T.W. Measurement of rill and ephemeral gully flow velocities and their model expression affected by flow rate and slope gradient. *J. Hydrol.* **2020**, *589*, 125172. [CrossRef]
29. Huang, Y.; Chen, X.; Li, F.; Zhang, J.; Lei, T.; Li, J.; Chen, P.; Wang, X. Velocity of water flow along saturated loess slopes under erosion effects. *J. Hydrol.* **2018**, *561*, 304–311. [CrossRef]
30. Liu, H.Q.; Yang, J.H.; Liu, C.X.; Diao, Y.F.; Ma, D.P.; Li, F.H.; Rahma, A.E.; Lei, T.W. Flow velocity on cultivated soil slope with wheat straw incorporation. *J. Hydrol.* **2020**, *584*, 124667. [CrossRef]
31. Zhuang, X.; Wang, W.; Ma, Y.; Huang, X.; Lei, T. Spatial distribution of sheet flow velocity along slope under simulated rainfall conditions. *Geoderma* **2018**, *321*, 1–7. [CrossRef]
32. Fu, B.; Wang, Y.; Zhu, B.; Wang, D.; Wang, X.; Wang, Y.; Ren, Y. Experimental study on rainfall infiltration in sloping farmland of purple soil. *Trans. CSAE* **2008**, *24*, 39–43.
33. Shen, E.; Liu, G.; Dan, C.; Shu, C.; Wang, R.; Liu, X.; Zhou, J.; Chen, X. Combined effects of rainfall and flow depth on the resistance characteristics of sheet flow on gentle slopes. *J. Hydrol.* **2021**, *603*, 127112. [CrossRef]
34. Nicosia, A.; Di Stefano, C.; Palmeri, V.; Pampalone, V.; Ferro, V. Flow resistance of overland flow on a smooth bed under simulated rainfall. *CATENA* **2020**, *187*, 104351. [CrossRef]
35. Shi, F.; Zhang, F.; Shen, N.; Yang, M. Quantifying interactions between slope gradient, slope length and rainfall intensity on sheet erosion on steep slopes using Multiple Linear Regression. *Sci. Total Environ.* **2024**, *908*, 168090. [CrossRef] [PubMed]
36. Zhang, Y.-B.; Zheng, F.-L.; Wu, M. Research progresses in agricultural non-point source pollution caused by soil erosion. *Adv. Water Sci.* **2007**, *18*, 132.
37. Wu, L.; Peng, M.; Qiao, S.; Ma, X. Assessing impacts of rainfall intensity and slope on dissolved and adsorbed nitrogen loss under bare loessial soil by simulated rainfalls. *CATENA* **2018**, *170*, 51–63. [CrossRef]

38. Zhao, L.; Fang, Q.; Hou, R.; Wu, F. Effect of rainfall intensity and duration on soil erosion on slopes with different microrelief patterns. *Geoderma* **2021**, *396*, 115085. [CrossRef]
39. Li, X.; Zhang, Y.; Ji, X.; Strauss, P.; Zhang, Z. Effects of shrub-grass cover on the hillslope overland flow and soil erosion under simulated rainfall. *Environ. Res.* **2022**, *214*, 113774. [CrossRef]
40. Ramos, M.C.; Lizaga, I.; Gaspar, L.; Quijano, L.; Navas, A. Effects of rainfall intensity and slope on sediment, nitrogen and phosphorous losses in soils with different use and soil hydrological properties. *Agric. Water Manag.* **2019**, *226*, 105789. [CrossRef]
41. Tao, W.; Wu, J.; Wang, Q. Mathematical model of sediment and solute transport along slope land in different rainfall pattern conditions. *Sci. Rep.* **2017**, *7*, 44082. [CrossRef] [PubMed]
42. Gutiérrez, M.; Biagioni, R.N.; Alarcón-Herrera, M.T.; Rivas-Lucero, B.A. An overview of nitrate sources and operating processes in arid and semiarid aquifer systems. *Sci. Total Environ.* **2018**, *624*, 1513–1522. [CrossRef]